Int J Adv Manuf Technol (2017) 92:15–24
DOI 10.1007/s00170-017-0107-6

ORIGINAL ARTICLE

Design and evaluation of high-pressure nozzle assembly for laser cutting of thick carbon steel

S. Marimuthu[1,2] · A. K. Nath[3] · P. K. Dey[1] · D. Misra[1] · D. K. Bandyopadhyay[1] · S. P. Chaudhuri[1]

Received: 3 September 2016 / Accepted: 25 January 2017 / Published online: 15 February 2017

Abstract Laser cutting of carbon steel is extensively used across a range of industries, due to its advantage of high speed, low kerf and high quality. Currently, a 1-kW carbon dioxide (CO_2) laser with its subsonic nozzle assembly can be used only to cut steel plates up to around 10 mm. This paper aims to design and evaluate a high-pressure supersonic laser cutting nozzle assembly, which can enable a 1-kW CO_2 laser to cut steel of up to 50 mm thickness. Basic gas dynamic and compressible flow equations were used to design the supersonic nozzle assembly. The flow of the high-pressure gas jet inside the nozzle assembly was investigated using computational fluid dynamics (CFD), and the structural integrity of the high-pressure nozzle assembly was ensured using finite element analysis (FEA). The gas flow pattern at the exit of the nozzle assembly was computed and compared with the experimental observation made through a shadowgraph technique. Laser cutting experiments were performed with the developed supersonic nozzle assembly to demonstrate cutting of 50-mm-thick low carbon steel with 1-kW CO_2 laser.

Keywords CFD · FEA · Laser cutting · Supersonic nozzle · Shadowgraph · Thick steel cutting

✉ S. Marimuthu
marimuthusundar@gmail.com

[1] School of Laser Science and Engineering, Jadavpur University, Kolkata, India

[2] Manufacturing Technology Centre, Coventry, UK

[3] Department of Mechanical Engineering, Indian Institute of Technology, Kharagpur 721302, India

1 Introduction

Reactive fusion laser cutting of mild steel is extensively used in the manufacturing industries for cutting plates of various size and shapes. The cutting process is achieved through the energy from laser and exothermic reaction [1] of iron with oxygen. In conventional reactive fusion laser cutting process, the laser beam is focused onto the mild steel surface using a subsonic nozzle which also provides a low-pressure jet of oxygen. The oxygen gas reacts with steel at high temperature liberating heat as oxidation is exothermic in nature. The ensuing exothermic chemical reaction is then held in a thermodynamic balance between the heating effects of the laser and the cooling effect of thermal losses to the surrounding steel sheet [2].

Though laser cutting is one of the most used laser-based manufacturing process, the basic laser cutting process remained unchanged since its inception in the 1970s [3, 4]. Most existing and past research on laser cutting process focused predominantly on understanding the basic fundamentals and optimizing the laser cutting parameters [1, 2, 5, 6]. Powell et al. [1, 2] and Lin et al. [5] performed experimental and theoretical investigations on cut quality of laser cutting process. Few researchers [7, 8] have worked on thick section laser cutting. A dual-beam technique involving two 1.5-kW CO_2 lasers was used by Molian et al. [7] to cut thick steel and super alloy. Alfille et al. [8] compared the performance of pulsed Nd:YAG and CO_2 lasers for cutting thick metallic substances. High-power fibre laser is nowadays finding increased use in laser cutting and many researchers are attempting thick section cutting using high-power fibre lasers. Reactive fusion fibre laser cutting of 15-mm mild steel using 5-kW fibre laser was reported by Wandera [9].

It must be noted that most previous works on laser cutting involve use of low-pressure subsonic nozzle assembly, which

has significant restrictions on gas jet velocity and mass flow rate. The exothermic reaction between oxygen and iron is capable of generating massive energy [4] which was not fully utilized in the traditional laser cutting process due to the restrictions on mass flow rate associated with a low-pressure convergent nozzle. The subsonic gas jet restricts the mass flow rate, and subsequently, the power obtained through exothermic reaction is only around 20% of the total cutting power [4].

Supersonic nozzle showed improved laser cutting performance on both ferrous and non-ferrous metals. O′ Neil [10] first proposed the technology for laser cutting of thick steel that uses a high-pressure supersonic nozzle. His work demonstrated the potential of supersonic high-pressure oxygen jet for laser cutting of thick steel. After O′ Neil's work, many researchers [11, 12] investigated the fundamentals of supersonic laser cutting process of mild steel. Riveiro [13] used off-axis supersonic nozzle to enhance laser cutting of aluminium alloy (2024-T3). Riveiro showed that the supersonic gas jet helps in efficient removal of the melt produced during laser cutting thus controlling the dross formation during laser cutting of aluminium alloy.

This paper concerns design, fabrication and evaluation of a supersonic nozzle assembly that can be used for cutting 50-mm thick steel using a 1-kW CO_2 laser. The use of a high-pressure convergent-divergent nozzle will help to increase the exit gas velocity to supersonic velocity and with high mass flow rate. The increased mass flow rate of oxygen can be effectively used to increase the exothermic energy, and thus, thicker materials can be cut without increasing the laser power.

Structural and flow analyses are performed to evaluate the performance of the designed high-pressure nozzle assembly. Computational fluid dynamic (CFD) analysis was used to investigate the flow and pressure distribution inside the nozzle assembly. Finite element analysis (FEA) was carried out to verify the structural rigidity for the nozzle assembly. The flow characteristics of the exit gas jet from the nozzle predicted through the method of characteristic (MOC) and CFD analysis were compared with the actual flow pattern obtained by the shadowgraph technique. Few experiments for cutting materials of higher thickness were also conducted with the designed nozzle.

2 Design of supersonic nozzle assembly

Supersonic nozzle assembly can deliver oxygen at high velocity and mass flow rate, thereby, increasing the energy generated through exothermic reaction that can be effectively utilized to cut thick materials using a low-power laser source. The main criterion is to supply high volume of oxygen [4, 10] for the exothermic reaction and makes sure all the oxygen reacts with the iron to facilitate exothermic reaction. This is ensured by designing the nozzle optics, such that the diameter of laser beam print over the work piece surface is larger than the diameter of the gas jet, which ensures complete reaction of O_2 with iron. In this process, the power delivered by laser beam is used only to heat the work piece to the kindling temperature [1], whereas, the power produced by the exothermic reaction between O_2 and Fe is used for cutting. Moreover, a high-pressure supersonic nozzle can produce exit gas with better gas dynamic characteristics [14, 15]. Especially under the conditions of a correct design, the potential energy of the inlet pressure (P_0) is fully converted into kinetic energy, which also enhances the capability of removing the molten debris [16, 17].

The schematic diagram of the designed high-pressure nozzle assembly is shown in Fig. 1. The main parts of the assembly consist of a lens, a lens holder, nozzle chamber and convergent-divergent part of the supersonic nozzle. To adjust the focal position easily, the lens chamber body is divided into two main parts. The upper part is the lens holder and is fixed to the cutting head assembly, whilst the lower part has a sliding supersonic nozzle tip. The structure of the nozzle assembly is fully made up of copper for better dissipation of heat. The material properties of copper used to fabricate the nozzle assembly is given in Table 1. A CO_2 laser with a beam power of 1 kW was used as the laser source. The unfocused beam diameter was of 20 mm. A 50-mm focal length ZnSe plano-convex lens with 9.65 mm thickness was used to obtain a 3-mm-diameter laser beam spot at the work piece surface. The designed maximum pressure of the 9.65-mm-thick ZnSe lens is 16 bar. The focal point of the laser beam lies inside the nozzle assemble, close to the throat area of the supersonic nozzle tip.

The nozzle assembly is essentially a pressure cylinder, which converts pressure energy to kinetic energy. As the operating pressure of the nozzle assembly is higher, the structural and modal analyses become very important.

The nozzle assembly was considered as a thin shell and the wall thickness was calculated using Eqs. (1) and (2) [18]:

$$\text{Circumferential stress} = \frac{pD}{2t} \tag{1}$$

$$\text{Longitudinal stress} = \frac{pD}{4t} \tag{2}$$

where p is the pressure, D is the diameter and t is the thickness.

The nozzle wall thickness was calculated for a gas pressure of 7.5 bar (gauge pressure) with a factor of safety of 2. The throat and exit diameters of the supersonic nozzle were calculated based on one-dimensional gas dynamic formulations [19] given in Eqs. (3) and (4) as follows:

$$\left(\frac{A_0}{A_t}\right)^2 = \frac{1}{M^2}\left[\frac{2}{\gamma+1}\left(1+\frac{\gamma-1}{2}M^2\right)\right]^{(\gamma+1)/(\gamma-1)} \tag{3}$$

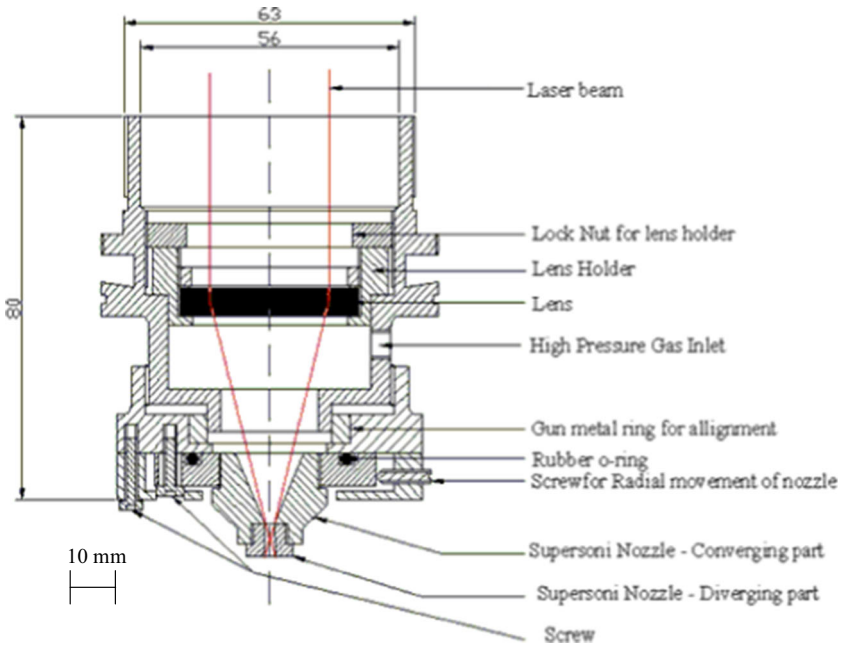

Fig. 1 Schematic diagram of nozzle assembly (all dimensions in mm)

where A_0 and A_t are the throat and exit area, M is the Mach number and γ is the specific heat ratio.

The mass flow rate equation is given by:

$$\rho VA = \text{constant and} M = \frac{V}{\sqrt{\gamma RT}} \tag{4}$$

where ρ is the density, V is the jet velocity, R is the gas constant, T is the temperature and A is the area.

Using Eqs. (3) and (4), the throat diameter and exit diameter were computed as 1.98 and 2.5 mm, respectively, for a design inlet pressure of 7.5 bar. The profile of the convergent-divergent part of the nozzle significantly influences the flow properties of the exit jet. The nozzle profile is designed based on MOC formulation [19]. MOC provides a technique for designing the contour of a supersonic nozzle for shock-free, isentropic flow, assuming the flow to be inviscid and does not form a boundary layer. A computer code is developed using MATLAB software for designing an axi-symmetric, straight minimum length nozzle (MLN), with a sharp throat corner. Characteristic lines and nozzle profile obtained using MOC are shown in Fig. 2.

Table 1 Physical properties of the material (copper) for nozzle assembly

Density	8900 kg/m^3
Young modulus	128 GPa
Yield stress	110 MPa
Poisson's ratio	0.36
Thermal conductivity	392.9 W/m K
Specific heat	385 J/kg K
Thermal expansion coefficient	16.5 μm/m^{0}c

3 Gas flow analysis inside nozzle assembly using computational fluid dynamics

CFD analysis enables to understand the flow characteristics inside the nozzle assembly and estimate the pressure conditions along the inner walls of the nozzle assembly. ANSYS CFX was used for the CFD analysis. The numerical scheme employed a finite volume method, adopting integral form of the conservation equations. The solution domain is subdivided into a finite number of contiguous control volumes and conservation equations are applied to every control volume. Surface and volume integrals are approximated using

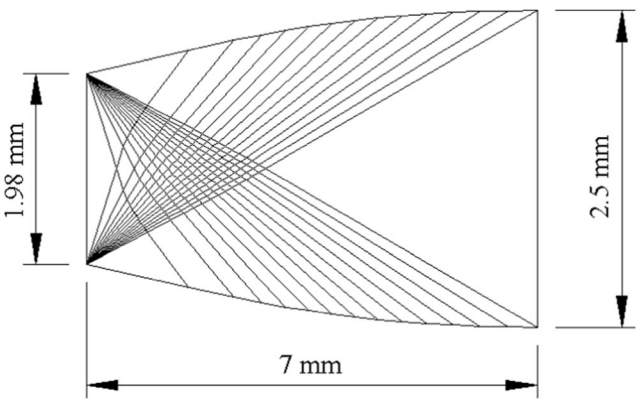

Fig. 2 Characteristic lines and contour of nozzle tip obtained through MOC (Mach number at exit = 1.98)

numerical quadrature. The mathematical formulation adopted is briefly described below.

The analysis is for steady state turbulent compressible flow. Based on Reynolds-averaged Navier–Stokes equations with the standard k–ε turbulence model, the governing equations describing the problem are as follows:

$$\frac{\partial \rho}{\partial t} + \nabla(\rho U) = 0 \tag{5}$$

$$\frac{\partial \rho U}{\partial t} + \nabla(\rho U \Theta U) - \nabla(\mu_{\text{eff}} \nabla U) - \nabla P' + \nabla(\mu_{\text{eff}} \nabla U)^T + B \tag{6}$$

where B is the sum of body force, μ_{eff} is the effective viscosity accounting for turbulence, P' is the modified pressure and $U\Theta U$ is the Reynolds stress.

$$\text{where } P' = P + \frac{2}{3}\rho k \tag{7}$$

The k–ε model, like the zero-equation model, is based on the eddy-viscosity concept, so that

$$\mu_{\text{eff}} = \mu + \mu_t \tag{8}$$

where μ_t is the turbulent viscosity.

The k–ε model assumes that the turbulent viscosity is linked to the turbulence kinetic energy and dissipation, via the relation

$$\mu_t = C_\mu \rho \frac{K^2}{\varepsilon} \tag{9}$$

where C_μ is a constant.

The values of k and ε come directly from the differential transport equations for the turbulence kinetic energy and turbulence dissipation rate:

$$\frac{\partial(\rho k)}{\partial t} + \nabla(\rho U k) = \nabla\left[\left(\mu + \frac{\mu_t}{\sigma_k}\right)\nabla k\right] + p_k - \rho\varepsilon \tag{10}$$

$$\frac{\partial(\rho \varepsilon)}{\partial t} + \nabla(\rho U \varepsilon) = \nabla\left[\left(\mu + \frac{\mu_t}{\sigma_\varepsilon}\right)\nabla \varepsilon\right] + \frac{\varepsilon}{k}(C_{\varepsilon 1} P_k - C_{\varepsilon 2}\rho\varepsilon) \tag{11}$$

where $C_{\varepsilon 1}$, $C_{\varepsilon 2}$, σ_k and σ_e are constants and P_k is the turbulence production due to viscous and buoyancy forces. The model constants $C_{1\varepsilon}$, $C_{2\varepsilon}$, C_μ, σ_k and σ_ε are assigned to the following values: $C_{1\varepsilon} = 1.44$, $C_{2\varepsilon} = 1.92$, $C_\mu = 0.09$, $\sigma_k = 1$ and $\sigma_\varepsilon = 1.3$.

One significant characteristic of turbulent flow is the transfer of momentum, heat and mass by means of molecular transport processes, namely, viscosity and diffusion. The conservation equations used for turbulent flows are obtained from those of laminar flows using the time averaging procedure commonly known as Reynolds averaging. For a turbulent flow, the characteristic variables, namely, pressure, velocity and temperature, may vary with both space and time.

$$\frac{\partial \rho h_{\text{tot}}}{\partial t} - \frac{\partial \rho}{\partial t} + \nabla(\rho U h_{\text{tot}}) = \nabla(\lambda \nabla T) + \nabla\left[\mu \nabla U + \nabla U^T - \frac{2}{3}\nabla U \delta U\right] \tag{12}$$

where h_{tot} is defined as the specific total enthalpy, which for the general case of variable properties and compressible flow is given in terms of the specific static (thermodynamic) enthalpy h by:

$$h_{\text{tot}} = h + \frac{1}{2}U^2 \tag{13}$$

The three-dimensional solid mesh model used for flow analysis for the whole nozzle assembly is shown in Fig. 3a. The mesh consists of 24,632 tetrahedral elements, with finer mesh along the convergent-divergent part of the nozzle (as variation of flow is expected to be higher at this region). The computational domain and boundary conditions used for the CFD analysis are shown in Fig. 3b. The inlet stagnation (or gauge) pressure was taken as 7.5 bar for computation and the outlet pressure was assumed to be atmospheric (as the jet is discharged freely in the atmosphere). Apart from inlet and outlet boundary surfaces, all other surfaces were assigned the adiabatic wall boundary condition with no slip. Compressible flow was considered.

The governing equations are assembled using a segregated solution [20] method. SIMPLE algorithm [21] was used for solving the equations. As the governing equations are nonlinear and coupled, several iterations of the solution loop are performed before a converged solution is obtained. The convergence criterion for all the CFD simulations was set to 10^{-6}. Solutions took nearly 900 iterations to attain convergence. An additional grid independence test was also made to confirm the convergence of the simulation.

Figure 4 show the CFD results for flow through high-pressure nozzle assembly. From these figures, it is well evident that the flow varies smoothly right from the inlet to the exit of the nozzle assembly without any shock formation inside the nozzle assembly. Figure 4a shows the velocity streamlines from the inlet to the exit of the nozzle assembly. As expected, the jet inside the nozzle shows a high momentum, good uniformity and tidy boundary.

Figure 4b, c shows the velocity and Mach number contour observed inside the high-pressure nozzle assembly. A velocity of 476 m/s and Mach number of 1.75 were noticed at the exit of the supersonic nozzle. The Mach number computed by the CFD analysis (1.75) is less than the values noticed with the method of characteristics (1.98) (Fig. 2), which is attributed to the consideration of turbulence and viscosity in the CFD analysis. The high-velocity gas jet from the subsonic nozzle can produce a high shear force which is expected to enhance the removal of melt and dross from the laser cutting zone. Also, the high gas jet velocity can increase the volume of oxygen

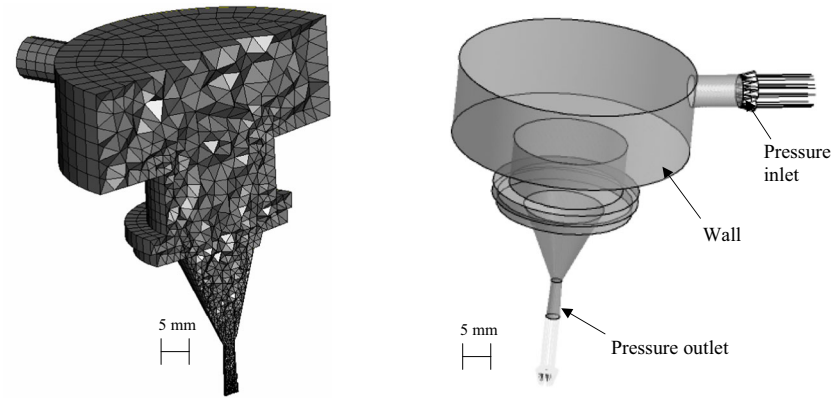

(a) Cross-section of the mesh used for CFD analysis

(b) Boundary conditions used for CFD analysis

Fig. 3 Details of the geometry and conditions used for CFD analysis. **a** Cross-section of the mesh used for CFD analysis. **b** Boundary conditions used for CFD analysis

supplied to the laser cut zone, thereby increasing the energy produced by exothermic reaction.

4 Finite element analysis of high-pressure nozzle assembly

The high-pressure nozzle assembly is basically a pressure vessel with a high-pressure differential between inside and outside walls. The high-pressure nozzle assembly must be designed carefully to cope with the operating pressure. Any rupture of the high-pressure nozzle assembly has the potential to cause extensive physical injury and property damage. The typical design of a high-pressure nozzle assembly component would entail looking at the geometry and manufacturing or construction details and subsequently at the loads experienced by the component. The load experienced [22] by the high-pressure nozzle assembly is related to factors such as operating pressure, operating temperature, and mechanical loads (due to dead weight) along with the postulated transients (typically those due to pressure).

The failures that the high-pressure nozzle assemblies are to be designed against are generally stress dependent [22]. For this reason, it becomes imperative to analyse the pattern of stress distribution in the high-pressure nozzle assembly. The operating stresses due to the imposed conditions can effectively be evaluated by finite element methods.

The requirements that are imposed on the structural design of the nozzle assembly are related to the operating pressure. The stress level is to be maintained below the allowable level, which is based on consideration of many failures like plastic collapse, fatigue, brittle fracture or buckling. Stress analysis involves determining the relationship between the applied loads and the associated response in terms of deflections, stresses and strains. The design procedures are based on linear elastic assumption, occasionally allowing for limited inelastic behaviour over a localized region. The basic equations used for finite element formulation are given below:

The stress-strain relation is given by

$$\{\sigma\} = [D]\{\varepsilon\} \tag{14}$$

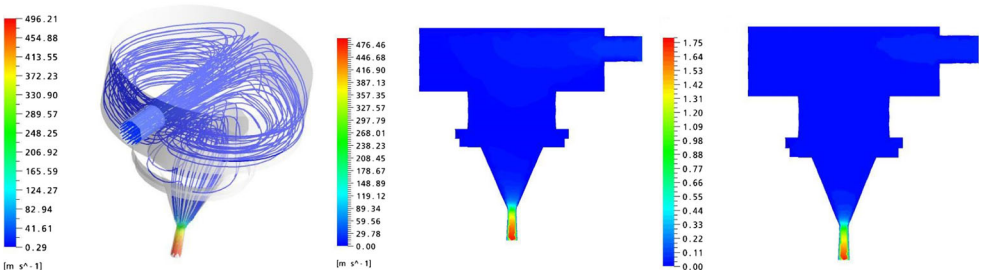

(a) Velocity streamlines inside the nozzle assembly

(b) Velocity distribution inside the nozzle assembly

(c) Variation of Mach number inside the nozzle assembly

Fig. 4 Results of the flow analysis inside the nozzle assembly. **a** Velocity streamlines inside the nozzle assembly. **b** Velocity distribution inside the nozzle assembly. **c** Variation of Mach number inside the nozzle assembly

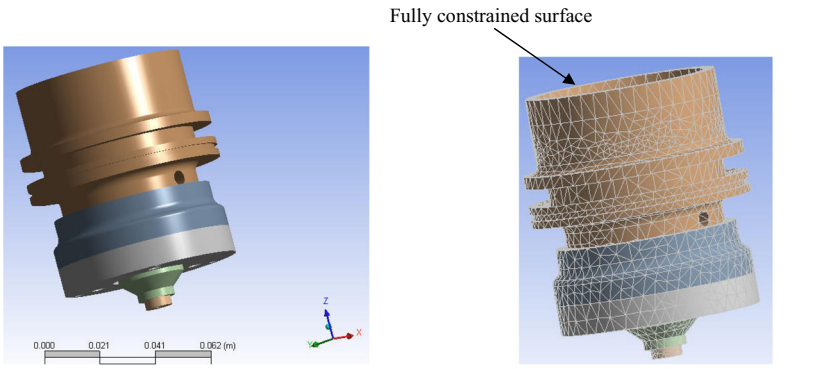

Fig. 5 Geometry and the mesh used for structural analysis of the nozzle assembly. **a** Geometry of the nozzle assembly. **b** Mesh used for structural analysis

(a) Geometry of the nozzle assembly (b) Mesh used for structural analysis

With stress vector $\{\sigma\} = \left[\sigma_X\, \sigma_y\, \sigma_Z\, \sigma_{XY}\, \sigma_{YZ}\, \sigma_{ZX}\right]^T$ (15)

And the total strain vector $\{\varepsilon\} = \left[\varepsilon_X\, \varepsilon_Y\, \varepsilon_Z\, \varepsilon_{XY}\, \varepsilon_{YZ}\, \varepsilon_{ZX}\right]^T$ (16)

ANSYS Multiphysics software was used to solve the FEA equations. The three-dimensional model used for the FE analysis was developed using Unigraphics NX modelling tool (Fig. 5a). Finite element meshing of the nozzle was done with three-dimensional, 10-node tetrahedral structural solid elements (SOLID 187). Convergence and grid sensitivity analyses were performed to choose the optimal mesh size. Figure 5b shows the mesh used for structural analysis which consists of 24,803 elements.

The pressure distribution obtained from the CFD analysis was imported to the ANSYS Multiphysics software and applied correspondingly over the inner surface of the nozzle assembly [20]. The shear force produced by the gas jet and the bolt loads are assumed to be negligible. The top surface of the nozzle assembly has been constrained as fixed support (Fig. 5b). Another important load induced in the nozzle assembly is the one produced due to the thrust of supersonic gas exit which is found using Eq. (17).

Force due to thrust = $\dot{M}(V_2 - V_1)$ (17)

Figure 6 shows the finite element result of the nozzle assembly. The Fig. 6a shows the von Mises stress distribution along the mid cross-section of the high-pressure nozzle assembly. As seen from the Fig. 6a, the maximum stress induced is 5.8 MPa which is significantly less than the yield stress of the material (100 MPa). The maximum stress was observed around the gas inlet area. Figure 6b, c shows the USUM displacement as the three-dimensional structure and in the mid cross-section. The maximum displacement of the nozzle assembly is in microns (0.65 μm) and well within the acceptable limit. As can be seen from this figure, the maximum deflection was observed around the convergent part of the supersonic nozzle.

Though the high-pressure nozzle is a static body, the modal analysis becomes important due to high-pressure gas flow

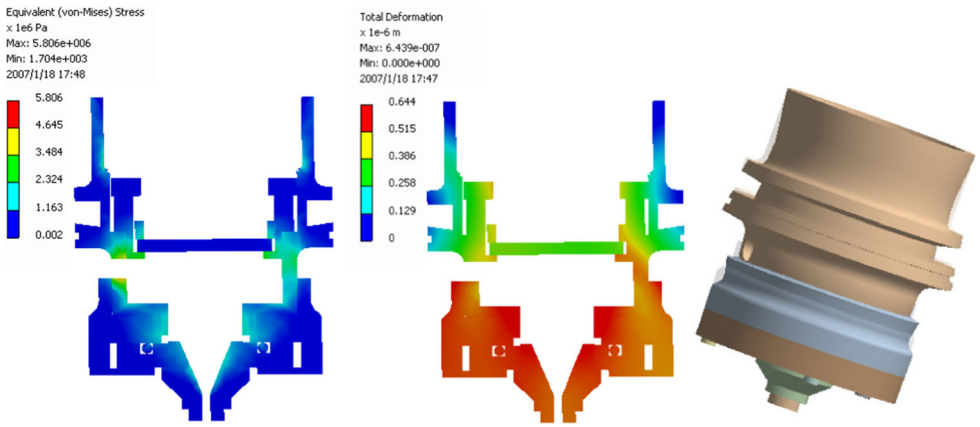

Fig. 6 Stress distribution and deformation of the nozzle assembly. **a** von Mises stress distribution along nozzle. **b** Total distortion along nozzle cross-section. **c** Deformed shape of the nozzle assembly

(a) von Mises stress distribution along nozzle cross-section (b) Total distortion along nozzle cross-section (c) Deformed shape of the nozzle assembly

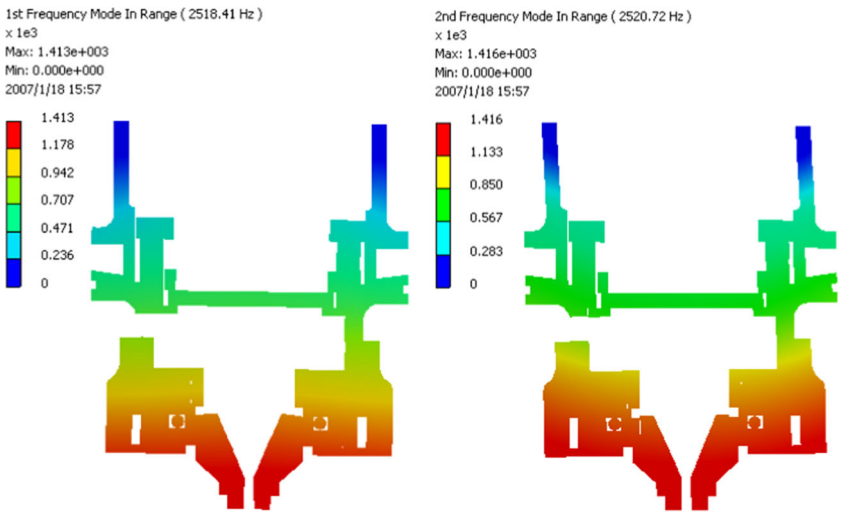

(a) First frequency mode (b) Second frequency mode

Fig. 7 Frequency modes observed for the high-pressure nozzle assembly. **a** First frequency mode. **b** Second frequency mode

from the exit of the nozzle. Natural frequencies are properties of a system, and it is important to study the natural frequencies and corresponding mode shapes of a system. If a forcing frequency is applied to the system near to or at the natural frequency, resonance can occur. In the following investigation, the flexural vibration modes of the nozzle assembly were studied, and hence, only the components of displacements in the top are fixed (as shown in Fig. 5b).

The first four natural frequencies obtained using the modal analyses for the high-pressure nozzle are 2.518, 2.520, 5.099 and 6.669 MHz, respectively. It is interesting to note that for certain modes, the Eigen values and hence the frequencies are repetitive in nature. This is due to the symmetry of the nozzle structure. Modes 1 and 2 have the same frequency, and looking at their corresponding mode shapes in Fig. 7a, b, respectively, it is noticed that they are of the same shape but bending at mutually perpendicular planes.

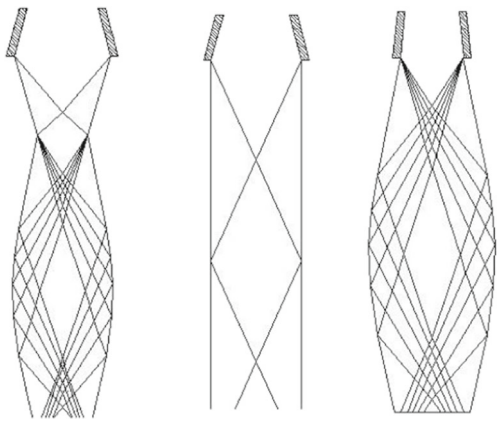

(a) 3.0 bar (b) 7.5 bar (c) 12 bar

Fig. 8 Gas jet patterns from the exit of the nozzle for various stagnation pressure (P_0) with design stagnation pressure of 7.5 bar. **a** 3.0 bar. **b** 7.5 bar. **c** 12 bar

5 Characteristic of the exit gas jet from the nozzle assembly

MOC and CFD were used to analyse the characteristics of the exit gas jet under conditions of high inlet gas pressure. The characteristic of the exit gas jet has significant influence on the laser cut quality.

5.1 Exit gas jet analysis using method of characteristic

MOC is based on the following assumptions: the flow of the gas jet is two dimensional, irrotational, isentropic and supersonic; the fluid is a perfect gas, i.e. the viscosity and gravity forces are negligible; and the jet flow is steady and uniform. The analysis was performed only for the first periodic wave of the gas jet from the nozzle tip as this portion significantly influences the cutting performance. The characteristics and

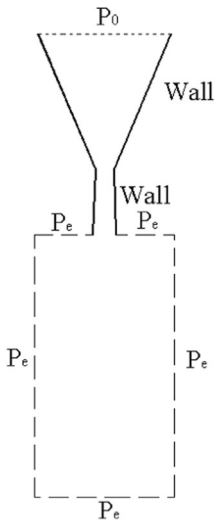

Fig. 9 Computational domain and boundary conditions used to investigate the exit gas jet

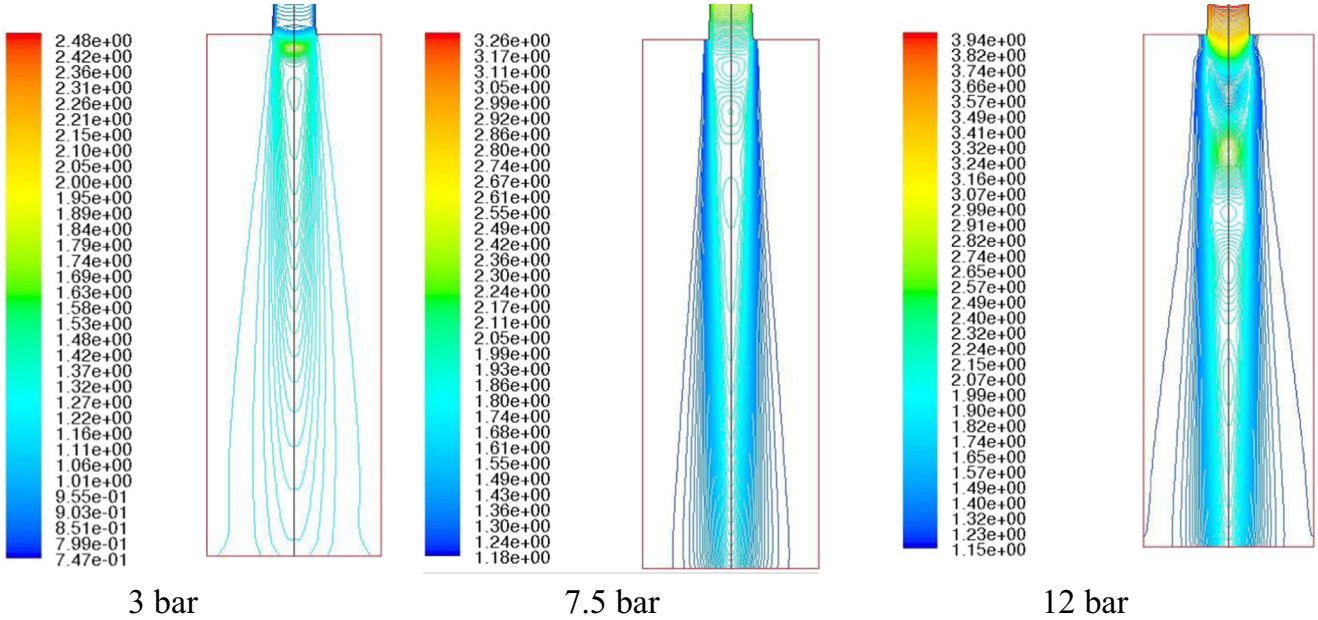

Fig. 10 CFR results of the exit gas flow pattern observed for various stagnation pressure (contour shows the density values in kg/m^3)

patterns of a supersonic jet escaping from the nozzle tip are mainly affected by the pressure ratio (P_e/P_0). The value of the exit gas pressure (P_e) can be calculated using Eq. (18).

$$P_e = \left(1 + \frac{k-1}{2} M_e^2\right)^{-(K/(K-1))} \text{x } P_o \tag{18}$$

Figure 8 shows the profile of the exit gas jet obtained through MOC. It is clear from Fig. 8b that the exit gas jet shows a uniform distribution, high momentum and parallel boundary when the stagnation inlet pressure is equal to its design pressure. This condition is much suitable for laser cutting operations. If the stagnation pressure is less than the design pressure (Fig. 8a), the gas jet behaves as an under-expanded jet. In this case, the cutting pressure and the thrust depend on the stand-off distance. The exit jet becomes over-expanded jet if the stagnation pressure is greater than the design pressure (Fig. 8c). Also, a strong shock is noticed at the end of the first expansion jet which causes energy loss and reduces the capability of removing the molten slag during cutting process.

5.2 Exit gas jet analysis using CFD

CFD analysis of the exit gas jet was performed using the finite volume-based FLUENT code to understand the gas jet characteristic from the high-pressure nozzle assembly. The two-dimensional axi-symmetric mesh was generated using Gambit software and the same was imported to FLUENT for analysis. Axi-symmetric steady-state compressible flow was assumed for the analysis. The governing equations were based on the Reynolds-averaged Navier–Stokes equations with the standard k–ε turbulence model.

The computation domain used for the analysis is shown in Fig. 9. P_0 is the inlet stagnation pressure and P_e is the exit pressure. The boundary conditions are treated as isentropic and the flow obeys ideal gas laws. The gas jet can expand freely from the supersonic nozzle to the atmosphere. The analysis was carried out for three different inlet stagnation pressures (3, 7.5 and 12 bar) with an ambient pressure of 1 atm at the outlet (P_e). Grid sensitivity analysis was performed prior to the analysis and converged results were obtained after 2000 iterations, approximately.

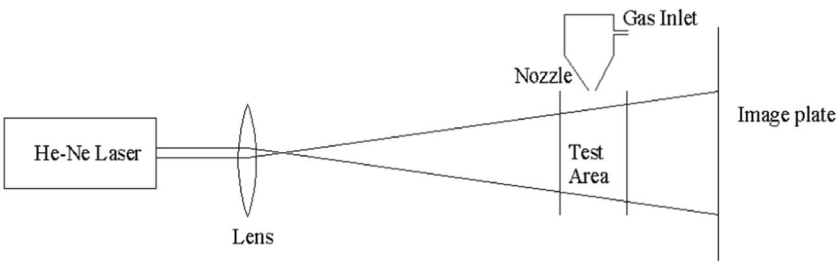

Fig. 11 Schematic diagram of shadowgraph arrangement used to visualize the exit gas jet

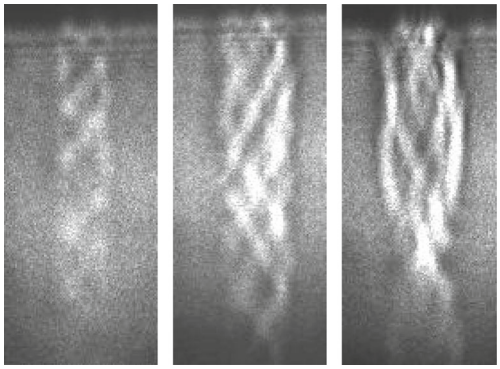

Fig. 12 Shadowgraph results of the exit gas flow pattern observed for various stagnation pressure

Density profiles of the free jets from the supersonic nozzle were computed for various inlet stagnation conditions and the results are shown in Fig. 10. As can be seen from the figure, inlet gas pressure of 7.5 bar results in the best gas jet characteristic, without any shock disc. However, shock formation was observed for 3 and 12 bar gas pressures.

5.3 Experimental exit gas jet visualization using shadowgraph

For high-speed liquid jets, effective experimental flow visualization is necessary to investigate the characteristics of the flow. It is widely recognized that optical flow visualization is the most suitable method to observe the shock waves in a compressible flow. Shadowgraph technique is the simplest optical visualizing procedure and it is especially convenient for observing the shock location in gas jet [23].

As illustrated in Fig. 11, a defocused He-Ne laser (wavelength of 632.8 nm) was used as a light source to illuminate the flow structure in the jet streams. Oxygen gas was used as the working fluid. Due to the immense change of gas pressure and density near the shock wave fronts of the gas flow, a clear shadowgraph can be projected onto the screen and captured by a CCD image system.

Figure 12 shows the shadowgraph results of the supersonic nozzle with stagnation pressures of 3, 7.5 and 12 bar, respectively. Under the process conditions as indicated in Fig. 12, the shock waves have been visualized and the shadowgraphs of shock wave were intensified with the increase of air pressure.

At the design pressure of 7.5 bar, the exit jet shows good flow properties as shown in Fig. 12. It can be found that the location of the shock waves moves downstream from the nozzle exit with increase of air pressure. As seen from the figure, Mach disc occurred at an entrance pressure greater than 7.5 bar in the present experiment. These shock discs will cause loss of energy which results in turbulence and loss of momentum. The shape of the first periodic wave is almost identical to that obtained from computer simulation, except that the length and the width of the first periodic wave are shorter and larger than those obtained from simulation shown in Figs. 8 and 10. The main reason is that the theory of two-dimensional steady gas dynamics is based on entropy continuity or enthalpy continuity without consideration of energy loss.

6 Thick section laser cutting trials using the developed high-pressure nozzle assembly

Cutting trials have been carried out to study the performance of the developed high-pressure nozzle assembly. A 1-kW CO_2 laser with TEM 01* beam has been used for the cutting process. Oxygen gas with an inlet stagnation pressure of 7.5 bar and mild steel plate of 50 mm thickness has been used for the cutting trials. The nozzle assembly has been aligned so that the beam and nozzle were concentric. The laser beam diameter was maintained to be 3 mm on the surface of the steel to ensure that the gas jet diameter (2.5 mm) was less than the laser foot print. Figure 13a shows a photograph of the cutting process operating under stable conditions, and Fig. 13b shows

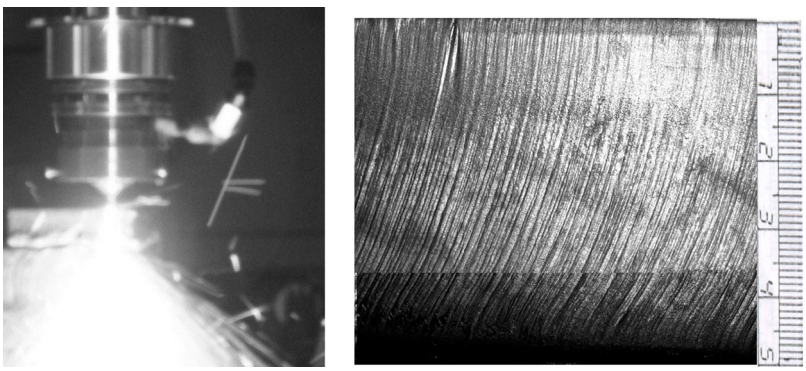

(a) Photograph showing cutting of 50 mm mild steel plate with 1 kW power

(b) Image showing the cut surface of 50 mm carbon steel

Fig. 13 Thick section laser cutting using the developed supersonic nozzle assembly. **a** Photograph showing cutting of 50-mm mild steel plate with 1 kW power. **b** Image showing the cut surface of 50-mm carbon steel

the cut surface of 50-mm mild steel with oxygen pressure of 7.5 bar, laser power of 1 kW and speed of 320 mm/min.

7 Conclusions

Numerical and experimental investigations were carried out to understand the performance of the designed supersonic laser cutting nozzle assembly. The developed supersonic laser cutting nozzle was successfully used for thick section laser cutting of carbon steel. The following conclusions are drawn from the study:

1. A 1-kW CO_2 laser along with a supersonic nozzle assembly can be used to cut 50-mm thick steel at a speed of 340 mm/min and gas pressure of 7.5 bar.
2. FEM results show that the stress, strain and displacement values of the designed nozzle assembly were within the allowable limits.
3. The designed supersonic nozzle assembly exhibits good gas dynamic characteristics under designed operating pressure. Supersonic nozzle shows good flow characteristics inside and outside the nozzle assembly with good uniformity in pressure, momentum and density distribution and without any shock waves.
4. Strong capability of dross removal and large tolerance to variation of stand-off and other process parameters can be achieved using supersonic nozzle assembly, and this would enhance the quality and capability of laser cutting process.

Acknowledgements The authors gratefully acknowledge the financial support (Sanction No. 2004/34/3-BRNS) provided by the Board of Research in Nuclear Sciences, DAE, India, for carrying out this research work. The cutting experiment with high-power CW CO2 laser was performed at Raja Ramanna Centre for Advanced Technology, Indore, Madhya Pradesh, India.

References

1. Powell, J. and A. Kaplan (2004) Laser cutting: from first principles to the state of the art. In Proceedings of the 1st Pacific International Conference on Application of Lasers and Optics, Melbourne
2. Powell J et al (2011) Fibre laser cutting of thin section mild steel: an explanation of the 'striation free'effect. Opt Lasers Eng 49(8): 1069–1075
3. Sullivan A, Houldcroft P (1967) Gas-jet laser cutting. Br Weld J 14(8):443–445
4. Powell J (1993) CO2 laser cutting, vol 214. Springer-Verlag, Berlin
5. Li L, Sobih M, Crouse P (2007) Striation-free laser cutting of mild steel sheets. CIRP Annals-Manufacturing Technology 56(1):193–196
6. Teixidor D, Ciurana J, Rodriguez CA (2014) Dross formation and process parameters analysis of fibre laser cutting of stainless steel thin sheets. Int J Adv Manuf Technol 71(9–12):1611–1621
7. Molian P (1993) Dual-beam CO2 laser cutting of thick metallic materials. J Mater Sci 28(7):1738–1748
8. Alfille JP, Pilot G, de Prunele D (1996) New pulsed YAG laser performances in cutting thick metallic materials for nuclear applications. In: Lasers, optics, and vision for productivity in manufacturing I. International Society for Optics and Photonics, pp 134–144
9. Wandera C, Kujanpää V, Salminen A (2011) Laser power requirement for cutting thick-section steel and effects of processing parameters on mild steel cut quality. Proc Inst Mech Eng B J Eng Manuf 225(5):651–661
10. O'Neill W, Gabzdyl JT (2000) New developments in laser-assisted oxygen cutting. Opt Lasers Eng 34(4–6):355–367
11. Sundar M et al (2009) Effect of process parameters on the cutting quality in lasox cutting of mild steel. Int J Adv Manuf Technol 40(9):865–874
12. Zhang C et al (2016) Evaluation and optimal design of supersonic nozzle for laser-assisted oxygen cutting of thick steel sections. Int J Adv Manuf Technol:1–9
13. Riveiro A et al (2011) Effects of processing parameters on laser cutting of aluminium–copper alloys using off-axial supersonic nozzles. Appl Surf Sci 257(12):5393–5397
14. Fieret J, Terry MJ, Ward BA (1986) Aerodynamic interactions during laser cutting. In: Proceedings of SPIE 0668, Laser Processing: Fundamentals, Applications, and Systems Engineering, vol 53. doi: 10.1117/12.938884
15. Ward, B. (1984) Supersonic characteristics of nozzles used with lasers for cutting. Proceedings of ICALEO, Boston p. 94–101
16. Man H, Duan J, Yue T (1997) Design and characteristic analysis of supersonic nozzles for high gas pressure laser cutting. J Mater Process Technol 63(1):217–222
17. Man H, Duan J, Yue T (1998) Dynamic characteristics of gas jets from subsonic and supersonic nozzles for high pressure gas laser cutting. Optics & Laser Technology 30(8):497–509
18. John H, Harvey P (1991) Theory and design of pressure vessels. Van Nostrand Reinhold, New York
19. Anderson JD (1990) Modern compressible flow: with historical perspective, vol 12. McGraw-Hill, New York
20. ANSYS help documentation. (2013) ANSYS, Inc. Theory Release. 14
21. Patankar, S. (1980) Numerical heat transfer and fluid flow. CRC press
22. Matthews, C. (2001) Engineers' guide to pressure equipment. Professional Engineering Publishing Limited, London and Bury St Edmunds, UK, ISBN. 1(86058298): p. 2
23. Masuda W, Nakamura T (1993) Effects of nozzle contour on the aerodynamic characteristics of underexpanded annular impinging jets. JSME International Journal Series B 36(2): 238–244